Tuneable resonance properties of graphene by nitrogen-dopant

Haifei Zhan[a], Ye Wei[b] and Yuantong Gu[c]

School of Chemistry, Physics and mechanical Engineering, Queensland University of Technology, Brisbane, QLD 4109, Australia

[a]zhan.haifei@qut.edu.au, [b]ye.wei@qut.edu.au, [c]yuantong.gu@qut.edu.au

Keywords: graphene, nitrogen-dopant, resonance, molecular dynamics simulation, natural frequency, quality factor

Abstract. Doping as one of the popular methods to manipulate the properties of nanomaterials has received extensive application in deriving different types of graphene derivates, while the understanding of the resonance properties of dopant graphene is still lacking in literature. Based on the large-scale molecular dynamics simulation, reactive empirical bond order potential, as well as the tersoff potential, the resonance properties of N-doped graphene were studied. The studied samples were established according to previous experiments with the N atom's percentage ranging from 0.38%-2.93%, including three types of N dopant locations, i.e., graphitic N, pyrrolic N and pyridinic N. It is found that different percentages of N-dopant exert different influence to the resonance properties of the graphene, while the amount of N-dopant is not the only factor that determines its impact. For all the considered cases, a relative large percentage of N-dopant (2.65% graphitic N-dopant) is observed to introduce significant influence to the profile of the external energy, and thus lead to an extremely low Q-factor comparing with that of the pristine graphene. The most striking finding is that the natural frequency of the defective graphene with N-dopant's percentage higher than 0.89% appears larger than its pristine counterpart. For the perfect graphene, the N-dopant shows larger influence to its natural frequency. This study will enrich the current understanding of the influence of dopants on graphene, which will eventually shed lights on the design of different molecules-doped graphene sheet.

Introduction

Graphene has been witnessed with enormous breakthroughs in research as well as applications since its unexpected discovery in 2004 [1]. The record-breaking properties of graphene, such as supreme mechanical stiffness (Young's modulus as high as 1 TPa [2]), very high electron mobility [3] and many other enticing properties have opened up huge potential applications [4]. Doping as one of the popular method to manipulate the properties of nanomaterials has received extensive applications in deriving different types of graphene derivates that being utilized as energy conversion and storage components [5], biosensors [6], high-performance FET devices [7], and others [8]. There are two typical ways to synthesize dopant graphene [9], one is the electrical doping, such as the absorption of gas or metal (e.g., Ti, Fe, Pt). Another is the chemical doping, which introduces substitutional atoms or molecules into the carbon lattice of graphene. Different substantional atoms (e.g. N, B, S, and Si) or adsorbed molecules (e.g., toluene, NO2, HNO3, and benzyl viologen) on graphene sheets have been reported [10]. Within these derivates, researchers found decreased electrical conductivity and an improved on/off ratio [11], improved capacitance while applied as ultracapacitors [12], excellent selectivity and sensitivity for glucose [13], and many other enhanced properties.

A number of researches have been conducted recently, which however were usually emphasized on the electrical or chemical properties of dopant graphene. For instance, the interactions between metal nanoparticles (such as Au, Ag, Pt and Pd) and graphene were examined by employing the Raman spectroscopy [14, 15]. Based on the density functional theory (DFT) calculations, the structural and electrical properties of Pt, Fe, Al nanoparticles adsorbed on monovacancy defective graphene were explored [16, 17]. Recently, Wu et al. [18] found different doping properties of

Au-graphene system were induced by the chemical interactions between graphene and the different Au configurations. It is noticed that, the understanding of the mechanical performance, stability or durability of graphene with different dopants are still rare in literature, which however is critical for certain notable applications of dopant graphene, such as graphene-based flexible electronics [4], and applications in the tissue-engineering [19]. To note that, several atomicstic studies [20-23] have already been reported on graphene, which only focused on the tension properties. While a lot of experiments have been reported for the graphene being applied as resonators due to its ultrasensitive detection of mass, force, pressure and charge [24]. However, early researchers have reported the graphene-resonator exhibit an extremely low quality (Q) factor. For a 20 nm thick multilayer graphene sheet, the Q factor was found to range from 100 to 1800 as the temperate decreased from 300 K to 50 K. A high Q factor (up to 4000) was reported for the multilayer graphene oxide films [25].

Therefore, the aim of this paper is to investigate the resonance properties of dopant graphene. More specifically, the N-dopant graphene will be chosen as the testing sample, which has attracted a huge research effort in literature. The molecular dynamics (MD) simulation will be used to conduct this study, which has been frequently applied in investigating the mechanical properties of different nanomaterials [26, 27].

Numerical Implementation

The vibrational study is based on a series of large-scale MD simulations that were carried out on either perfect graphene with N-dopant or defective graphene with N-dopant, size of ~2×10 nm^2. For the perfect graphene layer, a randomly distributed N-dopant is introduced with the N-dopant percentage ranging from 0.38% to 2.65%. While for the defective graphene layer with vancies, the N-dopant percentage ranges from 0.38% to 2.93%. Different testing samples were established accroding to previous experimental works [7, 13, 28]. The popularly applied reactive empirical bond order (REBO) potential [29] was utilized to describe the atomic interactions for carbon-carbon, which has been shown to well represent the binding energy and elastic properties of graphene. The nitron-carbon interaction is described by the Tersoff potential, which has been applied by many researchers [30].

During each simulation, the graphene sheet was first relaxed to a minimum energy state using the conjugate gradient algorithm. We then used the Nose-Hoover thermostat [31, 32] to equilibrate the sample at 10 K (NVT ensemble) for 400 ps at a time step of 0.5 fs while holding the newly obtained length of the graphene layer fixed. Finally, the graphene layer was actuated by applying a sinusoidal velocity excitation $v(z) = \lambda \sin(ky)$ along the *z*-axis, where λ is the actuation amplitude (equals 2 Å/ps), and *k* equals π / L (here *L* is the effective length of the graphene layer which excludes the two fixed edges, see Fig. 1). The equations of motion are integrated with time using a Velocity Verlet algorithm [33]. As illustrated in Fig. 1, the two ends of the graphene layer was fixed in all three directions to mimic a doubly clamped configuration, and the *x* (width direction) and *y*-axes (length direction) are chosen as the zigzag and armchair directions, respectively. As reported by Kim and Park [34], the spurious edge modes of vibration plays an critical role in the considerably reduced Q-factor for single layer graphene. To discuss the impact on the spurious edge modes of the graphene layer from the presence of N-dopant, no periodic boundary conditions were utilized at any point during the simulation process (which provides a close mimic to the real working condition of a nanoresonator).

We also emphasize that the graphene layer was modelled using an energy-conserving (NVE) ensemble during the free vibration process following the velocity actuation, and that the applied velocity field increased the total potential energy by less than 0.01%, which ensures that the oscillations occur in the linear regime. The overall simulation methodology to study the oscillatory properties of the graphene layer is identical to that used previously for metal NWs [34-37]. All simulations were performed using the open-source LAMMPS code [38].

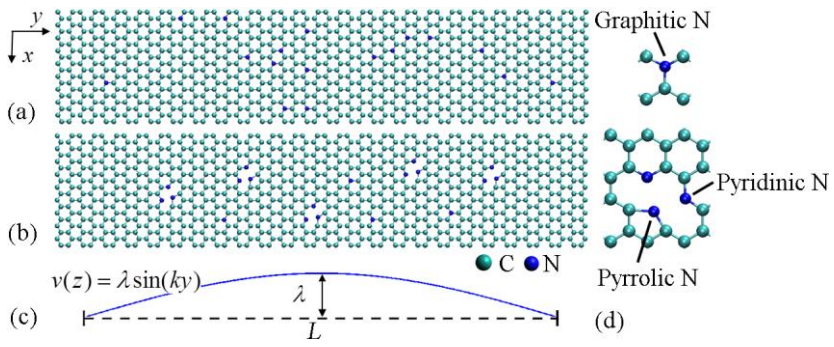

Fig. 1. (a) Simulation model of a doubly clamped graphene layer with randomly distributed N-dopant. (b) Simulation model of a doubly clamped defective graphene layer with N-dopant. Two edges were fixed in all directions, with the rest as the deformation region. (c) The profile of a sinusoidal velocity actuation. (d) Schematic representation of different N-dopant locations, including graphitic N, pyrrolic N and pyridinic N.

Results and Discussion

To acquire the impact from the N-dopant on the resonance properties of graphene, the Q-factor is defined as the ratio between the total system energy and the average energy loss in one radian at resonant frequency [39], i.e., $Q = 2\pi E / \Delta E$, where E is the total energy of the vibration system and ΔE is the energy dissipated by damping in one cycle of vibration. Assume Q-factor is constant during vibration, then after n vibration cycles, the maximum energy E_n is related to the initial maximum energy E_0 by $E_n = E_0(1-2\pi / Q)^n$ [40]. Since the energy-preserving (NVE) ensemble was adopted during the vibration, the loss of potential energy (*PE*) of the system must be converted to kinetic energy (*KE*). Thus, the time history of the external energy (*EE*) for the system will be tracked for the calculation of Q-factor, which is defined as the difference of *PE* before PE_0 and after PE_t the initial excitation is applied to the testing sample [35], i.e., $EE=PE_t-PE_0$.

Perfect graphene with N-dopant. Firstly, we investigated the resonance properties of graphene with randomly distributed graphitic N-dopant, with the N percentage ranging from 0.38% to 2.65% (comparable with the experimental results from Wang et al. [13]). Fig. 2a shows the time history of the external energy for a perfect graphene sheet. As is seen, the amplitude of the external energy decreases quickly with the increase of time, which indicates a large energy dissipation during vibration, thus a low Q-factor. Such evident energy dissipation is supposed as a result of the edge mode [34] that arises from atoms located at the two edges (see inset of Fig. 2b). After around 1000 ps vibration, the external energy of the system becomes much stable with its amplitude fluctuating around 0.2 eV. The corresponding frequency spectrum of the graphene sheet is derived by fast Fourier transformation. As shown in Fig. 2b, the natural frequency of the external energy is ~230 GHz. As the energy is a square function of the velocity, i.e., the natural frequency of the bilayer GS is half of the external energy frequency, or 115 GHz.

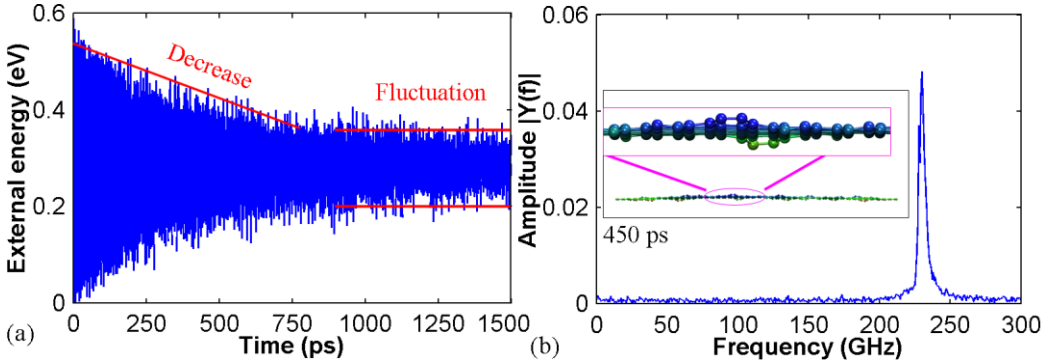

Fig. 2. Testing results from a pristine graphene sheet. (a) The time history of the external energy; (b) The frequency spectrum obtained from the fast Fourier transformation. Inset shows the graphene at 450 ps, and also reveals the edge modes of vibration (edge atoms vibrate differently).

We then considered the influence from randomly distributed N-dopant. Fig. 3a, 3b, 3c and 3d show the time history of the external energy of graphene with 0.88%, 1.77%, 2.15% and 2.65% N-dopant,

respectively. It is found that the pattern of these curves appears very similar with that of the pristine graphene sheet in Fig. 2a, i.e., the amplitude of the external energy decreases rapidly at the early vibration period and then arrives a stable value around 0.2 eV. More specifically, the external energy of the graphene with N-dopant percentage of 0.88% (Fig. 3a) and 2.15% (Fig. 3c) shows an earlier stable period, for which, the relative stable vibration period starts from 750 psec. While for the graphene with 1.77% N-dopant (Fig. 3b), this specific time appears around 1000 psec, same as observed from the perfect graphene sheet. This observation indicates that a higher Q-factor will be deduced for the graphene with 1.77% N-dopant comparing with that of the graphene with 0.88% N-dopant, i.e., the increase of the percentage of N-dopant is not necessary corresponding to a lower Q-factor and other factors (e.g., locations or distributions of the N-dopant) might also play a critical role in affecting the resonance properties of the graphene. With the further increase of the N-dopant percentage, a notable change of the external energy profile is observed. As illustrated in Fig. 3d, for the graphene with 2.65% N-dopant, a much sharp decrease of the external energy is observed with the stable vibration period starts as early as 250 ps, indicating a much lower Q-factor comparing with that of the pristine graphene sheet. Comparing all the studied cases, it is concluded that the presence of different N-dopant percentages will exert different influences to the resonance properties of the graphene. To further justify the influence from the N-dopant, different N-dopant types were studied in the following.

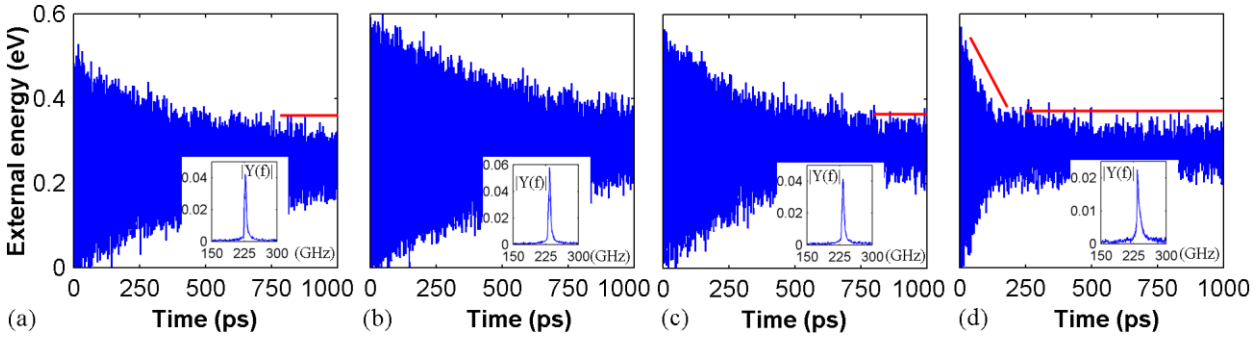

Fig. 3. Time history of the external energy obtained from perfect graphene sheet with the percentage of N-dopant as: (a) 0.88%; (b) 1.77%; (c) 2.15%; (d) 2.65%. Insets show the corresponding frequency spectrum.

Defective graphene with N-dopant. Different N-dopant types including graphitic N, pyridine-like N and pyrrole-like N were introduced to the graphene. These different dopant types were introduced to the defective graphene with the presence of vacancies. Different testing models were established according to the experimental reports by previous researchers [9]. One example of the testing samples is shown in Fig. 1b with 1.90% N-dopant. As illustrated in Fig. 4, the time history of the external energy for graphene with different percentages of N-dopant appears almost similar to each other, i.e., a relative rapid decrease at the beginning and arrives a stable vibration period after certain time (around 700 ps for the graphene with N-dopant percentage less than 1.90% and 750 ps for the graphene with 2.93% N-dopant). Therefore, it is further affirmed that the amount of N-dopant is not the only factor that influence the resonance properties of the graphene.

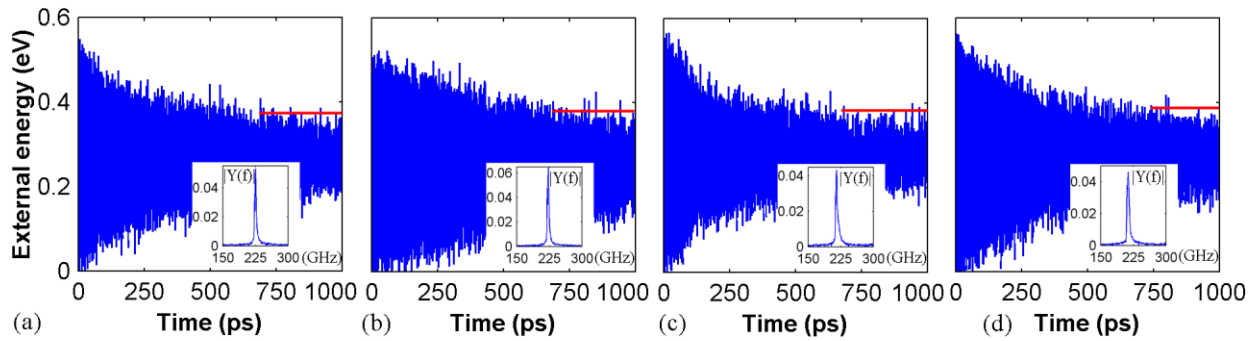

Fig. 4. Time history of the external energy obtained from defective graphene sheet with the percentage of N-dopant as: (a) 0.38%; (b) 0.89%; (c) 1.90%; (d) 2.93%. Insets show the corresponding frequency spectrum.

In the end, we compared the natural frequency that extracted from the MD simulation results for different testing samples. As compared in Fig. 5, the natural frequency exhibits a general decrease trend with the increase of graphitic N-dopant percentage, while an inverse trend is found for the defective graphene with N-dopant. The most striking finding is that the natural frequency of the defective graphene with N-dopant's percentage higher than 0.89% is larger than that obtained from the pristine defective graphene sheet. It is worthy to mention that the presence of N-dopant might also influence the edge mode of the graphene, which still requires further in-depth study.

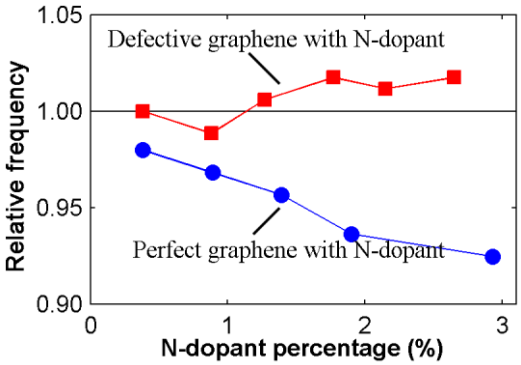

Fig. 5. Comparisons of the natural frequency estimated from the simulation results for graphene sheet with different percentages of N-dopant.

Conclusion

Basing on the MD simulation, the impacts on the resonance properties of graphene with N-dopant are studied in this paper. The N atom's percentage ranges from 0.38%-2.93% is considered, including three types of N dopant locations, i.e., graphitic N, pyrrolic N and pyridinic N. It is found that different percentages of N-dopant exert various influence to the resonance properties of the graphene, while the amount of N-dopant is not the only factor that determines its impact. For all considered cases, a relative large percentage of N-dopant (2.65% graphitic N-dopant) is observed to introduce significant influence to the profile of the external energy, and lead to an extremely low Q-factor comparing with that of the pristine graphene. The most striking finding is that the natural frequency of the defective graphene with N-dopant's percentage higher than 0.89% appears larger than its pristine counterpart. For the perfect graphene, the N-dopant shows larger influence to its natural frequency. This study will enrich the current understanding of the influence of dopants on graphene, which will eventually shed lights on the design of different graphene derivatives and their applications.

Acknowledgement

Support from the ARC Discovery Project (DP130102120) and the High Performance Computer resources provided by the Queensland University of Technology are gratefully acknowledged.

References

1. Novoselov, K., et al., *Electric field effect in atomically thin carbon films.* Science, 2004. **306**(5696): p. 666-669.
2. Lee, C., et al., *Measurement of the elastic properties and intrinsic strength of monolayer graphene.* Science, 2008. **321**(5887): p. 385-388.
3. Balandin, A.A., et al., *Superior thermal conductivity of single-layer graphene.* Nano Letters, 2008. **8**(3): p. 902-907.
4. Novoselov, K., et al., *A roadmap for graphene.* Nature, 2012. **490**(7419): p. 192-200.
5. Hou, J., et al., *Graphene-based electrochemical energy conversion and storage: fuel cells, supercapacitors and lithium ion batteries.* Physical Chemistry Chemical Physics, 2011. **13**(34): p. 15384-15402.
6. Artiles, M.S., C.S. Rout, and T.S. Fisher, *Graphene-based hybrid materials and devices for biosensing.* Advanced Drug Delivery Reviews, 2011. **63**(14): p. 1352-1360.
7. Wei, D., et al., *Synthesis of n-doped graphene by chemical vapor deposition and its electrical properties.* Nano Letters, 2009. **9**(5): p. 1752-1758.
8. Shin, H.J., et al., *Control of electronic structure of graphene by various dopants and their effects on a nanogenerator.* Journal of the American Chemical Society, 2010. **132**(44): p. 15603.

9. Wang, H., T. Maiyalagan, and X. Wang, *Review on recent progress in nitrogen-doped graphene: synthesis, characterization, and its potential applications.* Acs Catalysis, 2012. **2**(5): p. 781-794.
10. Lv, R. and M. Terrones, *Towards new graphene materials: Doped graphene sheets and nanoribbons.* Materials Letters, 2012.
11. Bokdam, M., et al., *Electrostatic doping of graphene through ultrathin hexagonal boron nitride films.* Nano Letters, 2011. **11**(11): p. 4631-4635.
12. Jeong, H.M., et al., *Nitrogen-doped graphene for high-performance ultracapacitors and the importance of nitrogen-doped sites at basal planes.* Nano Letters, 2011. **11**(6): p. 2472-2477.
13. Wang, Y., et al., *Nitrogen-doped graphene and its application in electrochemical biosensing.* ACS Nano, 2010. **4**(4): p. 1790-1798.
14. Jeon, K.J. and Z. Lee, *Size-dependent interaction of Au nanoparticles and graphene sheet.* Chemical Communications, 2011. **47**(12): p. 3610-3612.
15. Subrahmanyam, K., et al., *A study of graphene decorated with metal nanoparticles.* Chemical Physics Letters, 2010. **497**(1): p. 70-75.
16. Lim, D.H., A.S. Negreira, and J. Wilcox, *DFT Studies on the Interaction of Defective Graphene-Supported Fe and Al Nanoparticles.* Journal of Physical Chemistry C, 2011. **115**(18): p. 8961.
17. Lim, D.H. and J. Wilcox, *DFT-Based Study on Oxygen Adsorption on Defective Graphene-Supported Pt Nanoparticles.* The Journal of Physical Chemistry C, 2011. **115**(46): p. 22742-22747.
18. Wu, Y., et al., *Tuning the Doping Type and Level of Graphene with Different Gold Configurations.* Small, 2012.
19. Nair, R., et al., *Graphene as a transparent conductive support for studying biological molecules by transmission electron microscopy.* Applied Physics Letters, 2010. **97**(15): p. 153102-153102-3.
20. Reddy, C., et al., *Edge elastic properties of defect-free single-layer graphene sheets.* Applied Physics Letters, 2009. **94**(10): p. 101904-101904-3.
21. Pei, Q.X., Y.W. Zhang, and V.B. Shenoy, *Mechanical properties of methyl functionalized graphene: a molecular dynamics study.* Nanotechnology, 2010. **21**(11): p. 115709.
22. Pei, Q., Y. Zhang, and V. Shenoy, *A molecular dynamics study of the mechanical properties of hydrogen functionalized graphene.* Carbon, 2010. **48**(3): p. 898-904.
23. Zhang, Y., et al., *Mechanical properties of bilayer graphene sheets coupled by sp^3 bonding.* Carbon, 2011. **49**(13): p. 4511-4517.
24. Bunch, J.S., et al., *Electromechanical resonators from graphene sheets.* Science, 2007. **315**(5811): p. 490-493.
25. Robinson, J.T., et al., *Wafer-scale reduced graphene oxide films for nanomechanical devices.* Nano Letters, 2008. **8**(10): p. 3441-3445.
26. Mortazavi, B., et al., *Nitrogen doping and vacancy effects on the mechanical properties of graphene: A molecular dynamics study.* Physics Letters A, 2012. **376**(12): p. 1146-1153.
27. Lu, Q., W. Gao, and R. Huang, *Atomistic simulation and continuum modeling of graphene nanoribbons under uniaxial tension.* Modelling and Simulation in Materials Science and Engineering, 2011. **19**(5): p. 054006.
28. Deng, D., et al., *Toward N-doped graphene via solvothermal synthesis.* Chemistry of Materials, 2011. **23**(5): p. 1188-1193.
29. Brenner, D.W., et al., *A second-generation reactive empirical bond order (REBO) potential energy expression for hydrocarbons.* Journal of Physics: Condensed Matter, 2002. **14**(4): p. 783.
30. Kınacı, A., et al., *Thermal conductivity of BN-C nanostructures.* Physical Review B, 2012. **86**(11): p. 115410.
31. Hoover, W.G., *Canonical dynamics: Equilibrium phase-space distributions.* Physical Review A, 1985. **31**(3): p. 1695-1697.
32. Nosé, S., *A unified formulation of the constant temperature molecular dynamics methods.* The Journal of Chemical Physics, 1984. **81**: p. 511.
33. Verlet, L., *Computer 'experiments' on classical fluids. I. Thermodynamical Properties of Lennard-Jones Molecules.* Physical Review, 1967. **159**: p. 98-103.
34. Kim, S.Y. and H.S. Park, *The importance of edge effects on the intrinsic loss mechanisms of graphene nanoresonators.* Nano Letters, 2009. **9**(3): p. 969-974.
35. Kim, S.Y. and H.S. Park, *Utilizing mechanical strain to mitigate the intrinsic loss mechanisms in oscillating metal nanowires.* Physical Review Letters, 2008. **101**(21): p. 215502.
36. Zhan, H.F. and Y.T. Gu, *A fundamental numerical and theoretical study for the vibrational properties of nanowires.* Journal of Applied Physics, 2012. **111**(12): p. 124303-9.
37. Zhan, H., Y. Gu, and H.S. Park, *Beat phenomena in metal nanowires, and their implications for resonance-based elastic property measurements.* Nanoscale, 2012. **4**(21): p. 6779-6785.
38. Plimpton, S., *Fast parallel algorithms for short-range molecular dynamics.* Journal of Computational Physics, 1995. **117**(1): p. 1-19.
39. Bao, M.H., *Analysis and design principles of MEMS devices*2005: Elsevier Science.
40. Jiang, H., et al., *Intrinsic energy loss mechanisms in a cantilevered carbon nanotube beam oscillator.* Physical Review Letters, 2004. **93**(18): p. 185501.